Appl. Phys. B 78, 891–894 (2004)
DOI: 10.1007/s00340-004-1455-0

Applied Physics B
Lasers and Optics

Short-pulse, high-brightness X-ray production with the PLEIADES Thomson-scattering source

S.G. ANDERSON[1,✉]
C.P.J. BARTY[1]
S.M. BETTS[1]
W.J. BROWN[1]
J.K. CRANE[1]
R.R. CROSS[1]
D.N. FITTINGHOFF[1]
D.J. GIBSON[2]
F.V. HARTEMANN[1]
J. KUBA[1]
G.P. LeSAGE[1]
J.B. ROSENZWEIG[3]
D.R. SLAUGHTER[1]
P.T. SPRINGER[1]
A.M. TREMAINE[1]

[1] Lawrence Livermore National Laboratory, 7000 East Ave., Livermore, CA 94550, USA
[2] UCD Department of Applied Science, 661 Hertz Hall, Livermore, CA 94550, USA
[3] UCLA Department of Physics and Astronomy, 405 Hilgard Ave., Los Angeles, CA 90095, USA

Received: 28 October 2003/Revised version: 9 January 2004
Published online: 23 March 2004 •

ABSTRACT PLEIADES is a compact, tunable, high-brightness, ultra-short-pulse, Thomson-scattering X-ray source. Picosecond pulses of hard X-rays (10–200 keV) are created by colliding an ultra-relativistic (20–100 MeV), picosecond-duration electron beam with a high-intensity, sub-picosecond, 800-nm laser pulse. Initial operation of this source has produced 78-keV X-rays with 10^6 photons per pulse using a 57-MeV, 0.3-nC, 50-μm rms width electron beam and a 180-mJ, 15-μm rms width laser pulse. The angular distribution, energy, and energy spectrum of the source are found to agree well with theory and simulations. Source optimization is expected to increase X-ray output to between 10^7 and 10^8 photons per pulse with a peak brightness approaching 10^{20} photons/s/0.1% bandwidth/mm^2/mrad^2.

PACS 41.50.+h; 07.85.Fv; 41.75.Ht; 42.62.-b

1 Introduction

The use of short laser pulses and high-brightness, relativistic electron sources to generate high peak intensity, ultra-short X-ray pulses enables exciting new experimental capabilities. These include femtosecond pump–probe experiments used to temporally resolve material structural dynamics on atomic time scales [1], advanced biomedical imaging [2], and X-ray protein crystallography [3].

PLEIADES (picosecond (ps) laser electron interaction for the dynamic evaluation of structures) is a next-generation Thomson-scattering X-ray source being developed at Lawrence Livermore National Laboratory (LLNL). This source generates X-rays by scattering a high-intensity, sub-ps, 800-nm laser pulse off a high-brightness photo-injector-generated electron beam at the LLNL 100-MeV linac.

The scattered laser photons are relativistically up shifted in frequency into the hard X-ray range and are emitted in a narrow cone about the electron-beam direction. The X-ray energy, E_x, is given by

$$E_\mathrm{x} = E_\mathrm{L} \frac{2\gamma^2 (1-\cos\varphi)}{1+\gamma^2\theta^2+a_0^2}, \tag{1}$$

where E_L is the laser photon energy, $\gamma = E/m_\mathrm{e}c^2$ is the normalized electron energy, φ is the angle between the laser and electron beams, θ is the observation angle, and a_0 is the normalized vector potential of the laser field. The X-ray energy is therefore tunable through the electron-beam energy, giving for PLEIADES (20–100-MeV electrons) a range of 10–200 keV X-ray pulses.

Thomson-scattering generation of sub-ps pulses of hard X-rays (30 keV) has previously been demonstrated at the LBNL (Lawrence Berkeley National Laboratory) Advanced Light Source injector linac, with X-ray-beam fluxes of 10^5 photons per pulse [4, 5]. In addition, Thomson X-rays have been created at the Naval Research Laboratory [6] and the BNL (Brookhaven National Laboratory) Accelerator Test Facility [7]. The LLNL source is expected to achieve fluxes between 10^7 and 10^8 photons for pulse durations of 100 fs to 5 ps, using interaction geometries ranging from 90° (side-on collision) to 180° (head-on collision). In this paper we describe the initial operation of this X-ray source in the 180° geometry, resulting in 5-ps X-ray bunches. Here 10^6 photons per pulse were generated with 78-keV peak energy. The angular distribution, energy, and energy spectrum of the X-ray pulses are found to agree well with the predictions of three-dimensional (3 D) simulations.

2 Predicted X-ray properties

The spatial and temporal dimensions of the Thomson-scattered X-ray pulse are determined by the overlap of the laser and electron beams at the interaction point. The expected X-ray production is calculated by integrating the emission probability per unit time, $\mathrm{d}N_\mathrm{x}/\mathrm{d}t$, given by

$$\frac{\mathrm{d}N_\mathrm{x}}{\mathrm{d}t}(t) = \sigma_\mathrm{T} c \left[1 - \boldsymbol{v}\cdot\boldsymbol{k}\right] \iiint_V n_\gamma(\boldsymbol{x}, t)\, n_\mathrm{e}(\boldsymbol{x}, t)\, \mathrm{d}V, \tag{2}$$

✉ Fax: +1-925/423-9438, E-mail: anderson131@llnl.gov

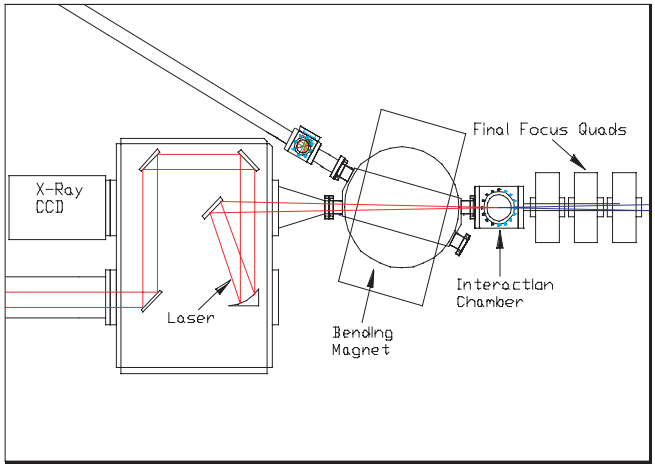

FIGURE 1 The PLEIADES interaction beamline

where N_x is the total number of X-rays produced, $n_\gamma(\boldsymbol{x}, t)$ is the laser photon density, $n_e(\boldsymbol{x}, t)$ is the electron density, σ_T is the total Thomson cross section, $\boldsymbol{v}$ is the velocity of the electron beam, and $\boldsymbol{k}$ is the wave number of the laser pulse. For 180° scattering, as depicted in Fig. 1, the integrated X-ray dose is found to scale as

$$N_x \propto \frac{N_e N_\gamma}{r_e^2 + r_L^2}, \tag{3}$$

where r_e and r_L are, respectively, the electron and laser beam spot sizes at the interaction point and N_e and N_γ are the total numbers of electrons and photons in the two beams.

While (3) reveals the scaling of the X-ray flux with beam intensities, a more rigorous treatment of this process must include the effects of a three-dimensional laser focus, as well as the energy spread and emittance of the electron beam. For this reason, the X-ray-production process was simulated using 3 D codes in both the time and frequency domains [9] to obtain integrated photon yield and spectral information. PARMELA [10] electron beam dynamics simulations from the photocathode to the interaction point were used to create realistic phase-space distributions, while $n_\gamma(\boldsymbol{x}, t)$ was assumed to be Gaussian in the transverse and longitudinal dimensions and the Rayleigh range of the laser focus was determined assuming a two-times diffraction-limited focus. These simulations predict an integrated photon yield of about 10^8, a spectral bandwidth of 10% on-axis, and a peak spectral brightness of approximately 10^{20} photons/s/0.1% bandwidth/mm^2/mrad^2.

It should be noted here that the discrepancy between this simulated photon yield and that achieved in the experiment (10^6) is primarily a result of a lower emittance, and 5 times smaller beam size, predicted by PARMELA simulations than those produced in the accelerator. As will be discussed below, simulations using the measured electron and laser beam parameters agree well with the observed X-ray properties.

3 Experimental procedure

The PLEIADES facility consists of a Ti–sapphire laser system capable of producing bandwidth-limited laser pulses of 50 fs with up to 500 mJ of energy at 800 nm, an S-band photocathode rf gun, and a 100-MeV linac consisting of four 2.5-m-long accelerator sections. The rf gun is designed to produce up to 1 nC of charge at 5 MeV [8]. The traveling-wave accelerator sections are then used to boost the electron beam to energies of 20–100 MeV. The electron bunch is generated at the copper photocathode by a picosecond, 300-μJ, UV laser that is synchronized to the interaction drive laser. In addition, the 2.8-GHz power that drives both the gun and the accelerator is derived by frequency multiplying the 81-MHz pulse train output signal of the mode-locked oscillator that seeds both the IR interaction laser and the UV photocathode drive laser. In this way the laser and electron beams are synchronized to the picosecond level required in this experiment.

A schematic of the interaction region is shown in Fig. 1. To maximize X-ray flux while minimizing effects of timing jitter, a laser incidence angle of 180 degrees with respect to the electron-beam direction was chosen for initial experiments, though a 90 degrees interaction geometry will also be possible in the future. The focal length between the final focus quadrupole triplet and the interaction region is 13 cm to allow for maximum focus strength and minimum electron bunch spot size. A 30-degrees dipole magnet is used to bend the electron bunch out of the X-ray-beam path following the interaction. This magnet also allows the measurement and tuning of the electron-beam energy and energy spread.

An off-axis, 1.5-m focal length parabolic mirror is used to focus the laser, which, assuming a diffraction-limited spot, should reach a minimum spot size of about 15 μm FWHM at the interaction point. Currently, a fused-silica flat mirror is placed in the X-ray-beam path to serve as the final steering optic for the laser, though there are plans to replace this with a beryllium flat, which will be more transparent to the X-ray beam.

To perform the spatial and temporal overlap, the interaction chamber also serves as a diagnostic chamber used for imaging and streak-camera analysis of the laser and electron bunches. The diagnostic used here consists of a polished alu-

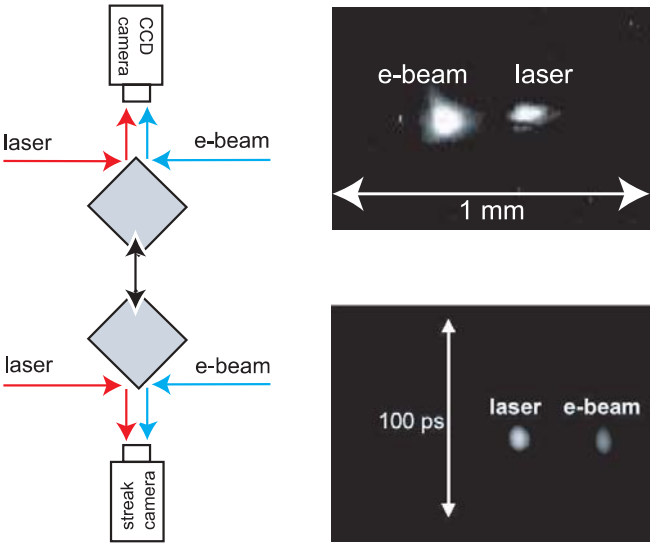

FIGURE 2 Spatial and temporal alignment diagnostic. *Above:* the cube is positioned to direct laser and OTR light to a CCD camera for spatial overlapping. *Below:* the cube position is altered to utilize the streak camera

Parameter	Value
Horizontal emittance ε_x	5 mm mrad (rms)
Vertical emittance ε_y	13 mm mrad (rms)
Spot size r_e	50 μm (rms)
Bunch length	7 ps (FWHM)
Charge	0.3 nC
Energy	57 MeV
Energy spread	0.2% (rms)

TABLE 1 Measured electron bunch parameters

Parameter	Value	Unit
Spot size r_L	35	μm (FWHM)
Duration	54	fs (FWHM)
Energy	180	mJ

TABLE 2 Measured laser pulse parameters

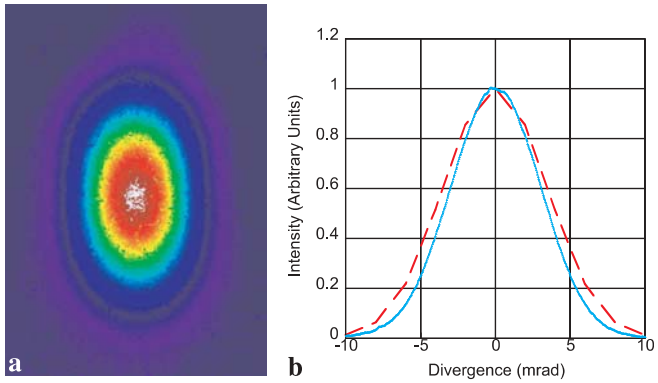

FIGURE 3 Measurement of X-ray-beam profile. **a** CCD image. **b** Horizontal line-out intensity profile data (*solid line*) and that predicted by simulation (*dashed line*)

minum cube mounted on a three-axis translation stage and aligned with the vertical faces intersecting the beamline at 45°, as shown in Fig. 2. This figure shows the method of timing synchronization of the laser and electron beams. Here optical transition radiation (OTR) [11] is generated by the electrons passing through the cube surface. The OTR light and the reflected laser light propagate together into a streak camera. The arrival time of the laser beam is adjusted with a delay arm to achieve the synchronization of the two beams shown in the streaked image in Fig. 2. The jitter has been measured to be within the resolution of the streak camera (about 2 ps), which is in agreement with indirect timing jitter measurements performed by mixing wake fields produced by the electron bunch with a frequency-multiplied photodiode signal from the laser oscillator.

The spatial alignment of the beams is done using the same diagnostic cube, but in this case by repositioning the cube such that the laser and OTR light are sent out through the opposite vacuum port to a CCD camera. In addition, the sizes of the electron and laser spots are measured with this method. To compare with the predictions of simulations, the electron and laser beam parameters of these experiments were measured and are given in Tables 1 and 2. The X-rays have been measured with a 16-bit CCD array fiber coupled to a cesium iodide scintillator. An X-ray photodiode and a germanium–lithium detector are also available for X-ray detection.

4 Experimental measurements

First light of the PLEIADES Thomson X-ray source was achieved in January 2003. Since that time, improvements in the laser energy and focus quality have resulted in more than an order of magnitude increase in X-ray flux. The electron and laser beam parameters of Tables 1 and 2 were achieved in September 2003 and used to generate the Thomson X-rays shown in Fig. 3a. Here, the beam profile has been measured with an X-ray CCD. The image was produced by integrating over 100 shots, and the peak photon energy was 78 keV. The average number of photons per shot is approximately 10^6, which agrees with simulation results using the experimental electron and laser beam parameters given in Tables 1 and 2.

The projected horizontal X-ray angular distribution is given in Fig. 3b, which shows an rms beam divergence of 3 mrad. The distribution compares well with the theoretical curve, which includes the broadening effects from the measured beam emittance and the narrowing effects derived from the spectral dependence of the transmission coefficient of the laser turning mirror. Note that, although not shown here, the vertical distribution also agrees with theoretical calculations. The broader vertical spot size is due to the effects of asymmetric electron-beam emittances and of laser polarization.

As (1) indicates, the X-ray energy spectrum is strongly correlated to the observation angle. Figure 4 shows a simulation illustrating this strong dependence. To observe this experimentally, a 0.005″ tantalum foil was placed in the X-ray-beam path. Tantalum has a k edge at 67.46 keV, and will therefore strongly attenuate X-rays slightly above that energy. Therefore, by varying the electron-beam energy, the X-ray spectrum will change, as will the profile of the transmitted beam.

The simulated X-ray profiles produced by 55- and 57-MeV electron beams, corresponding to 73- and 78-keV X-ray peak energies, respectively, are shown in Fig. 5. The measured profiles produced by these electron-beam energies are given in Fig. 6. As the figures show, the qualitative agreement

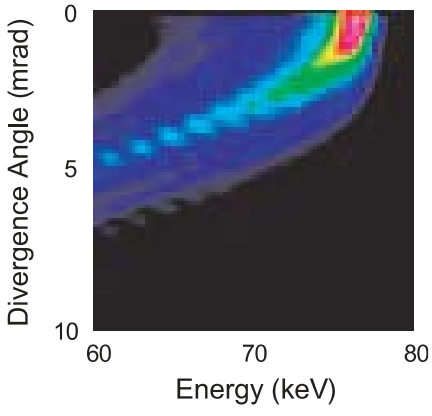

FIGURE 4 Simulation of the angular dependence of the X-ray spectrum

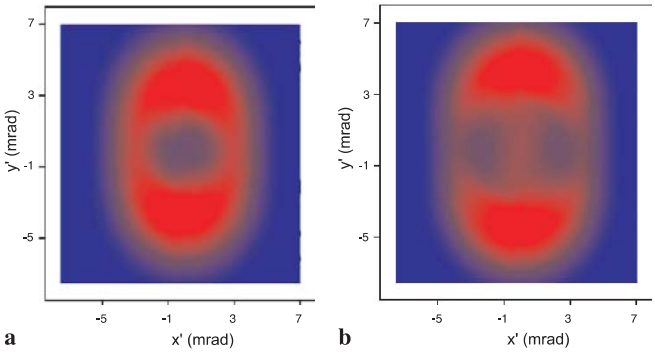

FIGURE 5 Simulation of X-ray transmission through a 0.005″ tantalum foil. **a** Distribution produced by a 55-MeV electron beam with a peak X-ray energy of 73.1 keV. **b** Distribution produced by a 57-MeV electron beam with a peak X-ray energy of 78.5 keV

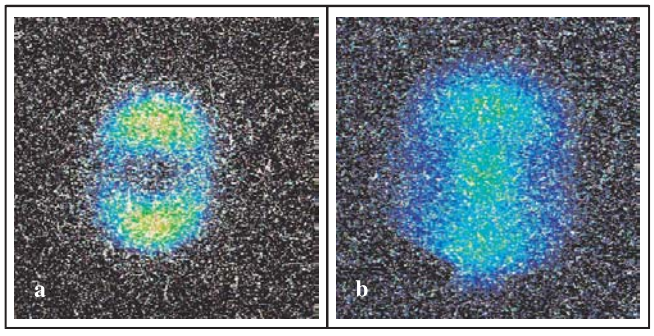

FIGURE 6 CCD images of the X-ray transmission through a 0.005″ tantalum foil. The electron-beam energies in parts **a** and **b** match those simulated in parts **a** and **b** of Fig. 5, respectively

between theory and measurement is quite good, indicating that the spectrum is consistent with expectations of this source.

5 Conclusions

The PLEIADES Thomson X-ray source is a unique, high-peak-brightness X-ray source that will be useful for ultra-fast imaging applications to temporally resolve material structural dynamics on atomic time scales. Electron-beam transport and X-ray-production simulations have been performed to completely model the theoretical source performance. These models have produced results consistent with experimental measurements in terms of integrated X-ray flux, angular dependence, and energy.

To date, 0.3-nC, 57-MeV bunches have been focused to 50-μm rms spot size and collided with a 180-mJ, 35-μm laser pulse to produce 10^6 X-rays per shot with 78-keV peak energy. Optimization of the experiment will include increasing the laser energy delivered to the interaction region to about 500 mJ and increasing the electron-beam focusing strength by an order of magnitude using a permanent magnet based system. These improvements will result in over 10^7 X-rays per pulse.

Additionally, decreasing the electron-beam emittance to less than 5-mm mrad rms by optimizing the UV laser profile and electron-beam transport will enable the achievement of a 10-μm spot size at the interaction and the production of 10^8 X-ray photons per pulse. Once optimization is complete, PLEIADES should achieve a peak X-ray brightness approaching 10^{20} photons/s/0.1% bandwidth/ $mm^2/mrad^2$.

ACKNOWLEDGEMENTS This work was performed under the auspices of the US Department of Energy by the University of California, Lawrence Livermore National Laboratory under Contract No. W-7405-Eng-48.

REFERENCES

1 C.W. Siders, A. Cavalleri, K. Sokolowski-Tinten, Cs. Tóth, T. Guo, M. Kammler, M. Horn von Hoegen, K.R. Wilson, D. von der Linde, C.P.J. Barty: Science **286**, 1340 (1999)
2 R. Fitzgerald: Phys. Today **53**, 23 (2000)
3 J. Drenth: *Principles of Protein X-ray Crystallography* (Springer, New York 1999)
4 R.W. Schoenlein, W.P. Leemans, A.H. Chin, P. Volfbeyn, T.E. Glover, P. Balling, M. Zolotorev, K.-J. Kim, S. Chattopadhyay, C.V. Shank: Science **274**, 236 (1996)
5 W.P. Leemans, R.W. Schoenlein, P. Volfbeyn, A.H. Chin, T.E. Glover, P. Balling, M. Zolotorev, K.J. Kim, S. Chattopadhyay, C.V. Shank: Phys. Rev. Lett. **77**, 4182 (1996)
6 A. Ting, R. Fischer, A. Fisher, C.I. Moore, B. Hafizi, R. Elton, K. Krushelnick, R. Burris, S. Jackel, K. Evans, J.N. Weaver, P. Sprangle, E. Esarey, M. Baine, S. Ride: Nucl. Instrum. Methods Phys. Res. A **375**, ABS68 (1996)
7 I.V. Pogorelsky, I. Ben-Zvi, T. Hirose, S. Kashiwagi, V. Yakimenko, K. Kusche, P. Siddons, J. Skaritka, T. Kumita, A. Tsunemi, T. Omori, J. Urakawa, M. Washio, K. Yokoya, T. Okugi, Y. Liu, P. He, D. Cline: Phys. Rev. ST Accel. Beams **3**, 090 702 (2000)
8 G.P. Le Sage, S.G. Anderson, T.E. Cowan, J.K. Crane, T. Ditmire, J.B. Rosenzweig: in *Advanced Accelerator Concepts: Ninth Workshop* (AIP, New York 2001) p. 391
9 F.V. Hartemann, H.A. Baldis, A.K. Kerman, A. Le Foll, N.C. Luhmann, Jr., B. Rupp: Phys. Rev. E **64**, 016501 (2001)
10 L. Young, J. Billen: Tech. Rep. LA-UR-96-1835, Los Alamos National Laboratory, 1996
11 L. Wartski, S. Roland, J. Lasalle, G. Filippi: J. Appl. Phys. **46**, 3644 (1975)